Investigating Timescales of Causality within Fluxes of Greenhouse Gasses

Sofía M. Swatt

ABSTRACT

In the context of anthropogenic perturbations to greenhouse gas concentrations, understanding the biophysical processes that modulate such gasses is essential in accurately modeling Earth's rapidly changing climate. Ecosystems are inherently nonlinear systems, in which the effects of causal variables cannot be separated or uncoupled from the variables that they influence. In order to uncover pathways of causality between variables, statistical methods must account for the associated asynchronous dynamics of time-delayed feedback loops that occur at different time scales. This study applies two algorithms for time-series analysis: (1) wavelet based time scale decomposition and (2) convergent cross mapping, in order to identify and quantify the extent to which contending environmental biophysical controls modulate fluxes of methane and carbon dioxide. Wavelet-decomposition and subsequent reconstruction of signals enabled isolated analysis at hourly, diel, multi-day, and seasonal time scales. These isolated signals were then inputted into a convergent cross mapping algorithm, for which the output correlation-coefficient was taken as the final quantifying parameter for causality. The following variables had the highest forcing capacity on methane flux at the (a) hourly, (b) diel, (c) multi-day, and (d) seasonal scale: (a,c) water vapor flux and (b,d) carbon dioxide flux. Analogously, the following variables had the highest forcing capacity on carbon dioxide flux: (a,b) water vapor flux, (c) methane flux, and (d) ecosystem respiration. Water vapor flux plays a dominant role in modulating fluxes of methane and carbon dioxide at shorter time scales, either directly via transpiration or indirectly via plant growth. At longer time scales methane flux is dominated by microbial populations and carbon dioxide flux is rooted in plant-mediated availability of oxygen. Wavelet decomposition proved to be a robust method for analyzing trends at different frequencies in a given signal, however, convergent cross mapping poses less reliability, in the context of noisy ecological data.

KEYWORDS

ecological time-series, information theory, eddy covariance, tidal wetland, biophysical controls

INTRODUCTION

The biogeochemical cycling of carbon between the biosphere, hydrosphere, and atmosphere, has fundamental implications for Earth's rapidly changing climate. Climate change is a multifaceted phenomenon, comprising abiotic and biotic factors that can amplify or intersect with the greenhouse gas effect. Whether a given ecosystem has a negative or positive radiative forcing (cooling or warming surface temperature) contribution to global warming, is ultimately contingent on the type of ecosystem, as the conditions which characterize each ecosystem determine the tendency for greenhouse gas sequestration or emission (De Deyn et al. 2008). Carbon dioxide (CO2) and methane (CH4), are the two dominant perturbed greenhouse gasses in terms of contemporary radiative forcing (Huntingford et al. 2015). Focusing on trace gas exchange and subsequent feedback of CO2 and CH4, across relevant terrestrial biomes that contain the cycling of these two gasses, is essential to better formulate global circulation models (Li et al. 2021). Trace gas exchange can be quantified based on fluxes, and measured using the eddy-covariance system (Liu et al. 2022). In the context of current-day carbon sequestration efforts, it is critical to understand how and which biophysical variables drive the fluxes of CO2 (FCO2) and CH4 (FCO4) across different environmental conditions and vegetation types, in order to perform accurate climate modeling for future increases in surface temperature (Li et al. 2021).

Tidal wetland ecosystems are of particular interest when considering FCO2 and FCH4 as they sequester carbon over the long-term. Long-term cumulative carbon uptake is achieved through anaerobic conditions which protect existing soil carbon, while vegetation continues to sequester atmospheric CO2 (Valach et al. 2021). However, there exists a trade-off since the anaerobic conditions that reduce carbon loss from decomposition, also produce CH4 in inundated, fresh to brackish (slightly saline) wetlands (Valach et al. 2021). This being said, tidal wetlands have shown a high CO2-sequestration-to-CH4-emission ratio (Callaway et al. 2012; Windham-Myers et al. 2020), and are correlated to negative radiative forcing (Arias-Ortiz et al. 2021). Wetlands contain the largest terrestrial carbon stores, therefore understanding the drivers of FCO2 and FCH4, which constitute overall carbon uptake and output, is imperative to predicting how these ecosystems will behave in a rapidly warming climate (Valach et al. 2021). In general wetland ecosystems, the variables that have been found to influence FCO2 include:

ecosystem respiration, solar radiation, precipitation, air temperature, and water vapor flux density (Sturtevant et al. 2016). Variables that influence FCH4 in wetland ecosystems are less linearly identifiable, as these processes vary in coupling strength in the short term and long term (Liu et al. 2022). For example, the main *seasonal* drivers of FCH4 are soil and water temperature, but the main *multi-day* driver of FCH4 is water table height (Sturtevant et al. 2016). Thus, time scales of causality must be additionally taken into consideration. It is critical that applied statistical methods account for the asynchronous processes that modulate fluxes of CO2 and CH4 in wetlands.

Applied statistical methods must accurately quantify the level of causality for biophysical variables that drive FCO2 and FCH4, and depict at which time scales there is causality. Multispatial convergent cross-mapping (CCM) is a recently-developed algorithm that can be used as a test for causal associations between pairs of processes in a given time-series (Clark et al. 2015). A time-series is a set of observations represented sequentially in time, in uniform intervals, and time-series decomposition allows us to isolate the trends embedded in a time-series signal at different time scales. Wavelet-based decomposition, specifically, is the most suitable decomposition method for revealing periodicities in signals that are non-stationary (varying in time) (Cazelles et al. 2008), which is the case in ecological systems comprising trace gas exchange. Two promising solutions to improving ecological modeling of FCO2 and FCH4 in wetlands are wavelet decomposition and convergent cross mapping, especially in the context of identifying causal associations between these fluxes and possible biophysical drivers.

The objective of this study is to investigate if wavelet-based time scale decomposition and convergent cross mapping can depict the timescales of causality within biophysical variables that modulate CH4 and CO2 fluxes in a tidal wetland ecosystem. The first aim is to apply wavelet-based decomposition to isolate major time scales of variation within a continuous time-series of FCO2 and FCH4, and each of their various contending biophysical drivers. The second is to apply CCM to identify and quantify scale-emergent causality between FCO2 and FCH4 and each biophysical variable.

METHODS

Study site

This study will analyze 170 days worth of bio-meteorological measurements starting September 2021, from Hill Slough, a freshwater tidal wetland located in the California Sacramento-San Joaquin River Delta.

Values for flux densities of greenhouse gasses: CO2 (FCO2) and CH4 (FCH4) were derived from the eddy covariance method, providing direct and continuous observations of the flux densities of these greenhouse gasses between the soil surface-atmosphere interface.

The specific continuous variables to compare with both FCH4 (gap-filled [nmol CH4 m^{-2} s^{-1}]) and FCO2 (gap-filled [umol CO2 m^{-2} s^{-1}]) are: water vapor flux [mmol H2O m^{-2} s^{-1}], gross primary productivity (gross photosynthesis estimated from Reichstein et al. 2005 [umol CO2 m^{-2} s^{-1}]), ecological respiration (ecosystem respiration estimated as performed in Reichstein et al. 2005 [umol CO2 m^{-2} s^{-1}]), air temperature [°C], air pressure [kPa], solar radiation (photosynthetically active radiation [umol m^{-2} s^{-1}]), water temperature at 2 different depths below the ground surface (10cm, 30cm) [°C], soil temperature at 4 different depths below the ground surface (0cm, 8cm, 16cm, 32cm) [°C], vapor pressure deficit [kPa], dissolved oxygen [mg L^{-1}], water vapor density [kg m^{-3}], water table height [cm], normalized difference vegetation index (half-hourly averages [index 0-1]), and conductivity (USGS NWIS at Jersey Island Dutch Slough site [microSiemens]).

Analysis

Wavelet-based time scale decomposition

Theory. Although Fourier analysis can be used to quantify constant periodic components in a time-series, it cannot characterize signals whose frequency content changes with time (Cazelles et al. 2008), which is the case in ecological systems. A wavelet transform decomposes a signal over functions (wavelets) that are narrow for high frequency signal properties and wide for low

frequency signal properties (Cazelles et al. 2008). Wavelets can be expressed as the function (φ) of time position (τ) and wavelet scale (*a*):

$$\varphi_{a,\tau}(t) = \frac{1}{\sqrt{a}}\varphi\left(\frac{t-\tau}{a}\right)$$

The wavelet transform of a time-series signal $x(t)$ is done by computing the integral of the product of the signal and the wavelet (φ) over continuous ranges of a and τ to get a wavelet coefficient $W_x(a,\tau)$ which represents the contribution of scale to the signal at different time positions (Cazelles et al. 2008). $W_x(a,\tau)$ is a large positive value if there is good matching between x and φ, a low value if the matching is low, and a large negative value if the matching is high but in the opposite phase of the wave. By doing so, the resulting wavelet coefficients comprise the reconstructed signal at each scale. The wavelet transform can be expressed as the following:

$$W_x(a,\tau) = \frac{1}{\sqrt{a}}\int_{-\infty}^{+\infty} x(t)\varphi^*\left(\frac{t-\tau}{a}\right)dt = \int_{-\infty}^{+\infty} x(t)\varphi^*_{a,\tau}(t)dt$$

where φ^* is the complex conjugate form of a wavelet, which only assumes positive frequencies within its range. By including the complex form of a wavelet, the resulting transform is less oscillatory than would be in the case of using a real wavelet (Prieto-Guerrero and Espinosa-Paredes 2019).

Application. In order to describe the temporal dynamics occurring at different time scales in the data, I applied maximal-overlap discrete wavelet transform (MODWT) in MATLAB Version 2020b (The MathWorks Inc. 2020) for the wavelet decomposition, with the Daubechies least-asymmetric wavelet filter ('sym4'). The MODWT package has been deemed advantageous for signal processing of gap-filled eddy-covariance flux measurements over traditional orthonormal discrete wavelet transform (ODWT), because of its high definition over various signal lengths and power preservation for multiresolution analysis (Liu et al. 2022). Each time-series was reconstructed for dyadic scales 1 (2^1 measurements = 1 hour) to 13 (2^{13} measurements = 170.7 days) (Sturtevant et al. 2016). Because patterns resulting from ecological processes naturally occur over a scale range rather than one specific scale, the reconstructed signals were summed over adjacent scales to analyze four general time scales of variation: Scales

1 and 2 (1–2 h) form the "hourly" scale , representing perturbations such as clouds passing overhead (Sturtevant et al. 2016). Scales 3–6 (4 h to 1.3 days) form the "diel" scale, representing the day-night cycle in sunlight and temperature (Sturtevant et al. 2016). Scales 7–10 (2.7–21.3 days) form the "multi-day" scale, identifying synoptic weather variability and variations in water table. Scales 11–13 (42.7–170.7 days) form the "seasonal" scale, representing the annual solar cycle and phenology (Sturtevant et al. 2016).

Convergent cross mapping to quantify causality

Theory. The CCM algorithm predicts the current quantity of one variable M_x using the time lags, or repeated delays in time between another variable M_y and M_x, and vice versa. M_x and M_y are projections of the true (unknown) system M, to each respective axis. The theory states that if M_x and M_y belong to the same dynamical system, the cross-mapping between them shall be convergent (Cao et al. 2021). In a system $Y = f(X,Y)$ cross-mapping signifies matching the values for M_x and M_y at the same time t. Convergence in CCM means that if X causes Y, then the longer an observation period, the increased accuracy of predicting Y using X. More specifically, since M_x and M_y are summaries of X and Y, M_x is then being used to predict Y. A high correlation between the CCM reconstruction and original data signifies a coupling interaction of X to Y, and acts as a proxy of causality. These correlation coefficients, delineated as cross mapping skill (ρ) can take values between -1 and 1 (Martin et al. 2019). The correlation coefficients are computed as the cosine of the angle between the predicted projected unit vectors where 1 represents a perfect correlation, 0 represents a complete failure of the reconstruction, and a hypothetical -1 would represent perfectly anti-correlated reconstruction vectors, which only occurs if the predicted values are exactly the opposite sign of the actual values (Martin et al. 2019).

Application. To identify and quantify scale-emergent causal interactions between each contending variable and FCO2 or FCH4, I applied CCM in R Studio (RStudio Team 2020), using the rEDM: Empirical Dynamical Modeling package, to each pair of time series signals for each of the 4 decomposed timescales. Time leads and lags are a necessary component to take into account in computing causal associations among a given pair of time series, as these forcing

dynamics in ecosystems are often phase-dependent and nonlinear. However, previous encounters with CCM have shown significant improvement in the algorithm's output accuracy when changing two parameters: the time lag and embedding dimension (Mønster et al. 2017). The optimal embedding dimension (E) for each time-scale was found using the 'simplex()' function in rEDM (E=5 hourly, E = 2 diel, E = 2 multi-day, E = 1 seasonal), however there is no function in rEDM for finding the optimal time lag. Therefore, based on the rEDM package description, the default optimal time lag (tp) was set -1 (Ye et al. 2019). This negative value of tp corresponds to estimating the past values of one time series, using the reconstructed states of the other time series. The subsequent outputs for cross mapping skill represent the extent to which one signal influences the other.

RESULTS

Wavelet based time scale decomposition

In applying maximal-overlap discrete wavelet transform (MODWT) in MATLAB for the wavelet decomposition, there were roughly 12000 output coefficients for each input time series signal (signals with NaN cells were replaced as empty cells). These coefficients represent the scaling of reconstructed wavelet transforms that were saved in a matrix of 12096 by 13, for each variables' time-series signal. The coefficients summed over adjacent scales ("hourly" scale 1-2, "diel" scale 3-6, "multi-day" scale 7-10, and "seasonal" scale 11-13) were then isolated as 4 separate vectors of length 12096 for each variable, to then be inputted into the CCM algorithm. Examples of the reconstructed wavelet transforms for FCH4 are in Figure 1. and for FCO2 in Figure 2. *See Appendix A for program detail.*

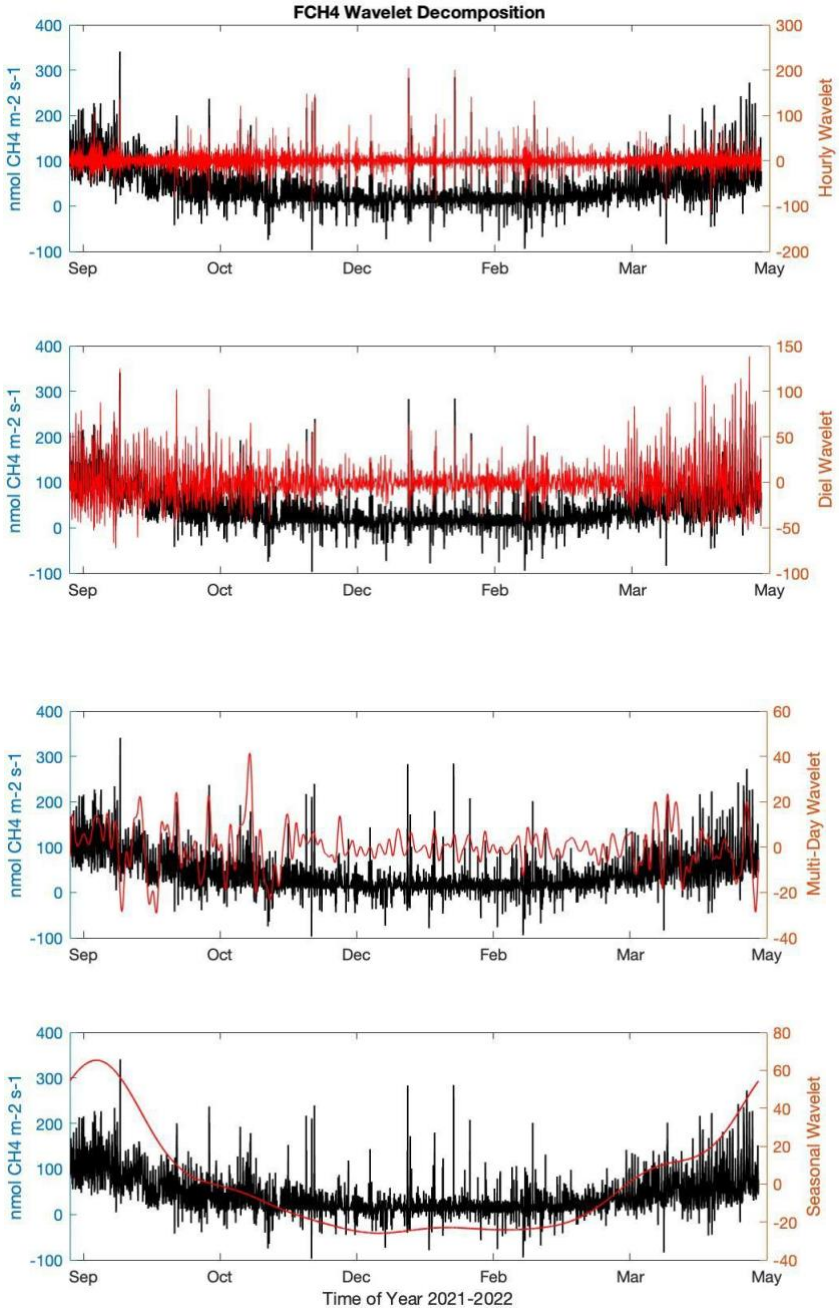

Figure 1. FCH4 variation isolated with wavelet decomposition at (a) hourly, (b) diel, (c) multi-day, (b) seasonal time scales. The red line indicates the wavelet detail reconstruction.

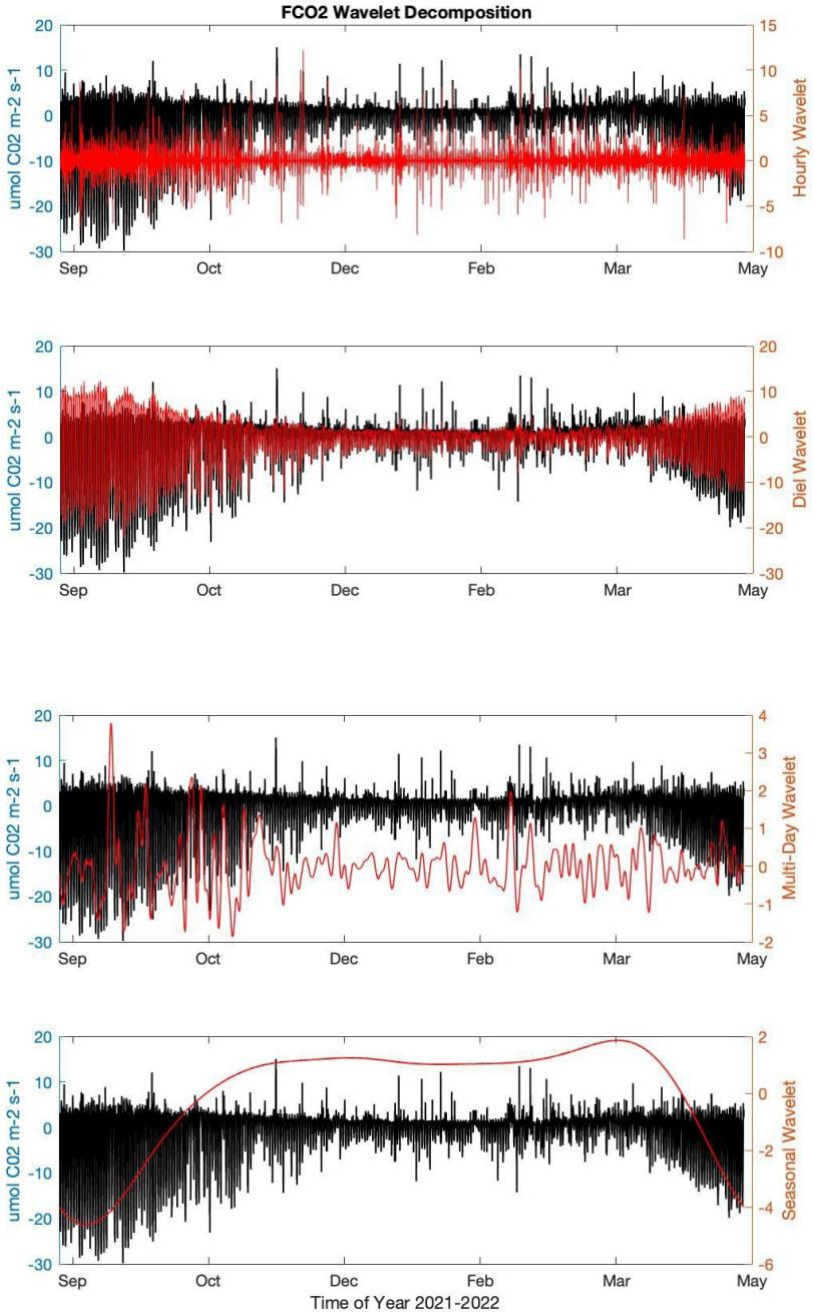

Figure 2. FCO2 variation isolated with wavelet decomposition at (a) hourly, (b) diel, (c) multi-day, (b) seasonal time scales. The red line indicates the wavelet detail reconstruction.

Convergent cross mapping to quantify causality

In applying rEDM: Empirical Dynamical Modeling package for the CCM analysis to all reconstructed wavelet transforms, the 'cross mapping skill' outputs were taken as a correlation coefficient. For both fluxes, the seasonal scale coefficients were greatest in magnitude compared to those of shorter timescales, and bi-directional forcing was exhibited by FCH4 (to FCO2), FCO2 (to FCH4), FH2O Vapor, and Ecosystem Respiration. *See Appendix B for program detail.*

FCH4

The primary drivers of FCH4 (Figure 3) were: FH2O Vapor (hourly and multi-day scales) and FCO2 (diel and seasonal scales). The following lists the CCM results in descending order for FCH4:

Hourly. The strongest biophysical causal relationships regarding FCH4 at the hourly scale were from FCH4 to FH2O Vapor, FH2O Vapor to FCH4, FCO2 to FCH4 and Ecosystem Respiration to FCH4. The negative correlations reflect how the predicted signal was opposite in sign to corresponding time-locations of the actual signal.

1. FCH4 xmap FH2O Vapor[1] (ρ = 0.179)
2. FH2O Vapor (ρ = 0.130)
3. FCO2 (ρ = 0.0593)
4. Ecosystem Respiration (ρ = 0.0249)
5. FCH4 xmap Ecosystem Respiration[1] (ρ = 0.0175)
6. Photosynthetic Radiation (ρ = 0.0131)
7. Water Temperature at 10cm depth (ρ = 0.00740)
8. Water Temperature at 30cm depth (ρ = 6.87E-03)
9. Dissolved Oxygen (ρ = 3.55E-03)
10. Soil Temperature at 16cm depth (ρ = 0)
11. Vegetation Index (ρ = 0.00)
12. Vapor Pressure Deficit (ρ = -0.000349)
13. Soil Temperature at 8cm depth (ρ = -0.00107)
14. Water Table Height (ρ = -0.00259)
15. Soil Temperature at 0cm depth (ρ = -0.00455)
16. Soil Temperature at 32cm depth (ρ = -0.00480)
17. Air Pressure (ρ = -0.00622)

[1] "xmap" is specified for FH2O Vapor and Ecosystem Respiration, which were the only variables that exhibited bidirectional forcing towards both FCH4 and FCO2

18. H2O Vapor Density (ρ = -0.00759)
19. Air Temperature (ρ = -0.00761)
20. Hydraulic Conductivity (ρ = -0.00880)

Diel. The strongest biophysical causal relationships regarding FCH4 at the diel scale were from FCO2 to FCH4, FH2O Vapor to FCH4, FCH4 to FH2O Vapor, and Photosynthetic Radiation to FCH4.

1. FCO2 (ρ = 0.369)
2. FH2O Vapor (ρ = 0.355)
3. FCH4 xmap FH2O Vapor[1] (ρ = 0.338)
4. Photosynthetic Radiation (ρ = 0.235)
5. Ecosystem Respiration (ρ = 0.151)
6. Soil Temperature at 16cm depth (ρ = 0.144)
7. Air Temperature (ρ = 0.137)
8. Vapor Pressure Deficit (ρ = 0.130)
9. Soil Temperature at 8cm depth (ρ = 0.116)
10. FCH4 xmap Ecosystem Respiration[1] (ρ = 0.105)
11. Soil Temperature at 0cm depth (ρ = 0.0908)
12. Water Table Height (ρ = 0.0850)
13. Soil Temperature at 32cm depth (ρ = 0.0661)
14. Water Temperature at 30cm depth (ρ = 0.0657)
15. Air Pressure (ρ = 0.0631)
16. Water Temperature at 10cm depth (ρ = 0.0405)
17. Hydraulic Conductivity (ρ = 0.0276)
18. H2O Vapor Density (ρ= 0.0148)
19. Dissolved Oxygen (ρ = 0.00732)
20. Vegetation Index (ρ = 0.00)

Multi-Day. The strongest biophysical causal relationships regarding FCH4 at the multi-day scale were from FH2O Vapor to FCH4, FCH4 to FH2O Vapor, FCO2 to FCH4, and H2O Vapor Density to FCH4.

1. FH2O Vapor (ρ = 0.500)
2. FCH4 xmap FH2O Vapor[1] (ρ = 0.406)
3. FCO2 (ρ = 0.286)
4. H2O Vapor Density (ρ = 0.285)
5. Vapor Pressure Deficit (ρ = 0.266)
6. Hydraulic Conductivity (ρ = 0.259)
7. Ecosystem Respiration (ρ = 0.243)
8. Soil Temperature at 8cm depth (ρ = 0.219)
9. Soil Temperature at 16cm depth (ρ = 0.207)

10. Air Temperature (ρ = 0.206)
11. Water Temperature at 10cm depth (ρ = 0.198)
12. Photosynthetic Radiation (ρ = 0.186)
13. Soil Temperature at 32cm depth (ρ = 0.185)
14. Soil Temperature at 0cm depth (ρ = 0.176)
15. Water Temperature at 30cm depth (ρ = 0.161)
16. FCH4 xmap Ecosystem Respiration[1] (ρ = 0.151)
17. Air Pressure (ρ = 0.124)
18. Water Table Height (ρ = 0.112)
19. Dissolved Oxygen (ρ = 0.0875)
20. Vegetation Index (ρ = 0.00)

Seasonal. The strongest biophysical causal relationships regarding FCH4 at the seasonal scale were from FCH4 to FH2O Vapor, FCO2 to FCH4, Air Temperature to FCH4, and Soil Temperature at 16 cm below the soil's surface to FCH4.

1. FCH4 xmap FH2O Vapor[1] (ρ = 0.927)
2. FCO2 (ρ = 0.926)
3. Air Temperature (ρ = 0.920)
4. Soil Temperature at 16cm depth (ρ = 0.882)
5. Ecosystem Respiration (ρ = 0.880)
6. Water Temperature at 10cm depth (ρ = 0.870)
7. Air Pressure (ρ = 0.870)
8. Soil Temperature at 32cm depth (ρ = 0.868)
9. FH2O Vapor (ρ = 0.838)
10. Vapor Pressure Deficit (ρ = 0.837)
11. Water Temperature at 30cm depth (ρ = 0.810)
12. FCH4 xmap Ecosystem Respiration[1] (ρ = 0.786)
13. Soil Temperature at 0cm depth (ρ = 0.783)
14. Soil Temperature at 8cm depth (ρ = 0.688)
15. H2O Vapor Density (ρ = 0.572)
16. Photosynthetic Radiation (ρ = 0.442)
17. Water Table Height (ρ = 0.113
18. Dissolved Oxygen (ρ = 0.0488)
19. Hydraulic Conductivity (ρ = 0.0231)
20. Vegetation Index (ρ = 0.00)

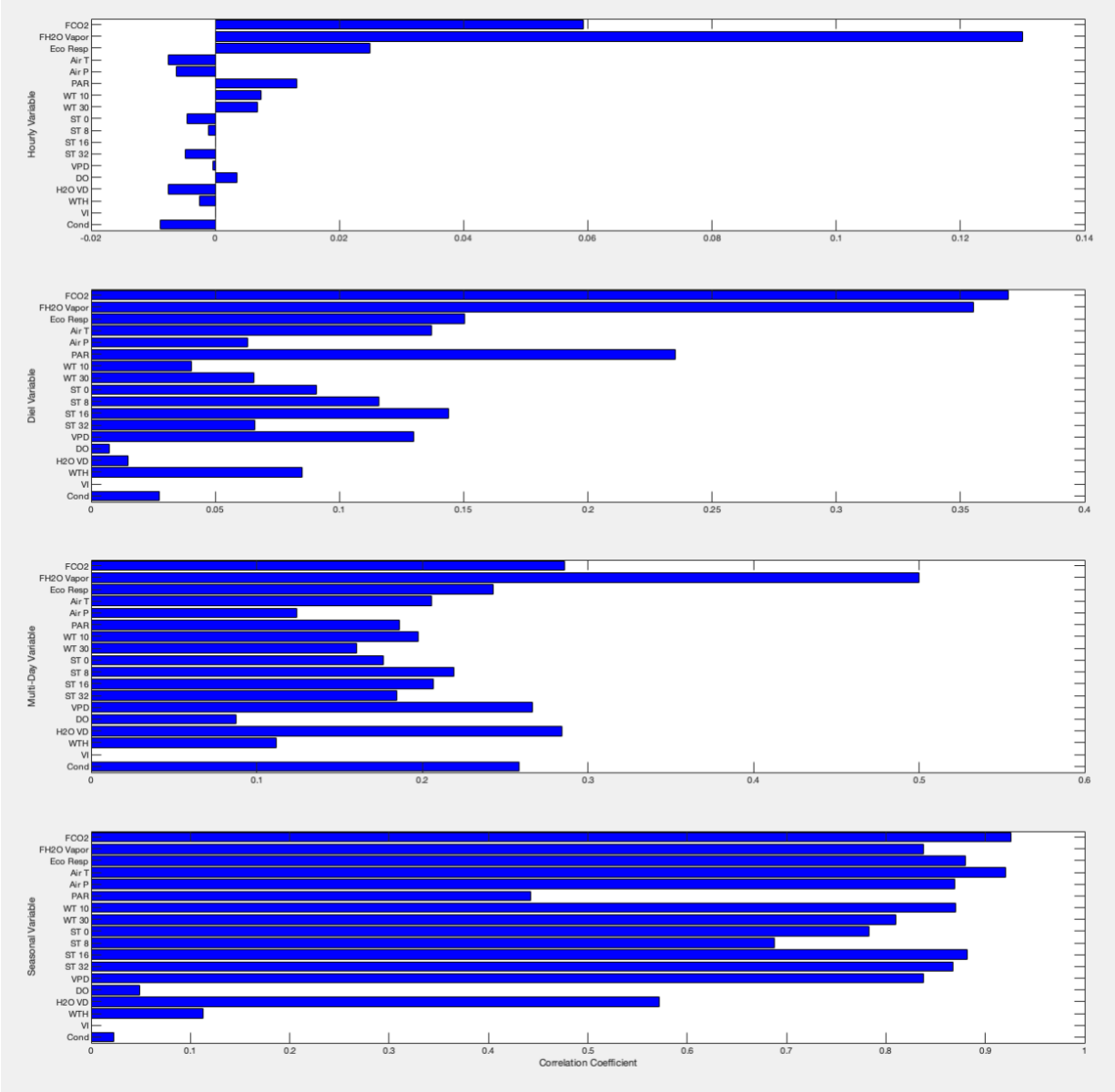

Figure 3. Causal Capacity of Contending Variables on FCH4. Applied rEDM package on contending biophysical drivers of FCH4. Cross Mapping Skill (ρ) represents correlation coefficients index (0-1). The closer ρ is to 1 is indicative of how much information from variable Y is stored in variable X, and thus how well X can predict Y, quantifying the level of causality from Y to X (Sugihara et al. 2012).

FCO2

The primary drivers of FCO2 (Figure 4) were: FH2O Vapor (hourly and diel scales), FCH4 (multi-day scale), and Ecosystem Respiration (seasonal scale). The following lists the CCM results in descending order for FCO2:

Hourly. The strongest biophysical causal relationships regarding FCO2 at the hourly scale were from FCO2 to FH2O Vapor, FH2O Vapor to FCO2, FCH4 to FCO2, and FCO2 to Ecosystem Respiration.

1. FCO2 xmap FH2O Vapor[1] (ρ = 0.146)
2. FH2O Vapor (ρ = 0.111)
3. FCH4 (ρ = 0.0486)
4. FCO2 xmap Ecosystem Respiration[1] (ρ = 0.0372)
5. Soil Temperature at 16cm depth (ρ = 0.0110)
6. Vapor Pressure Deficit (ρ = 0.00729)
7. Photosynthetic Radiation (ρ = 0.00684)
8. Dissolved Oxygen (ρ = 0.00355)
9. Soil Temperature at 32cm depth (ρ = 0.00228)
10. Water Temperature at 10cm depth (ρ = 0.000405)
11. Vegetation Index (ρ = 0.00)
12. Air Temperature (ρ = -0.000296)
13. Ecosystem Respiration (ρ = -0.000308)
14. Water Table Height (ρ = -0.00211)
15. Soil Temperature at 0cm depth (ρ = -0.00367)
16. Air Pressure (ρ = -0.00491)
17. Hydraulic Conductivity (ρ = -0.00531)
18. H2O Vapor Density (ρ = -0.00593)
19. Soil Temperature at 8cm depth (ρ = -0.00746)
20. Water Temperature at 30cm depth (ρ = -0.0100)

Diel. The strongest biophysical causal relationships regarding FCO2 at the diel scale were from FCO2 to FH2O Vapor, FH2O Vapor to FCO2, Ecosystem Respiration to FCO2, and FCO2 to Ecosystem Respiration.

1. FCO2 xmap FH2O Vapor[1] (ρ = 0.816)
2. FH2O Vapor (ρ = 0.803)
3. Ecosystem Respiration (ρ = 0.548)
4. FCO2 xmap Ecosystem Respiration[1] (ρ = 0.535)
5. Photosynthetic Radiation (ρ = 0.511)
6. Vapor Pressure Deficit (ρ = 0.468)
7. Air Temperature (ρ = 0.466)

8. Soil Temperature at 8cm depth (ρ = 0.394)
9. FCH4 (ρ = 0.377)
10. Soil Temperature at 16cm depth (ρ = 0.367)
11. Soil Temperature at 0cm depth (ρ = 0.324)
12. Soil Temperature at 32cm depth (ρ = 0.307)
13. Water Temperature at 30cm depth (ρ = 0.271)
14. Water Table Height (ρ = 0.254)
15. Air Pressure (ρ = 0.251)
16. Water Temperature at 10cm depth (ρ = 0.244)
17. Hydraulic Conductivity (ρ = 0.0773)
18. Dissolved Oxygen (ρ = 0.0228)
19. H2O Vapor Density (ρ = 0.0168)
20. Vegetation Index (ρ = 0.00)

Multi-Day. The strongest biophysical causal relationships regarding FCO2 at the multi-day scale were from FCH4 to FCO2, Vapor Pressure Deficit to FCO2, FH2O Vapor to FCO2, and Air Temperature to FCO2.

1. FCH4 (ρ = 0.369)
2. Vapor Pressure Deficit (ρ = 0.281)
3. FH2O Vapor (ρ = 0.274)
4. Air Temperature (ρ = 0.264)
5. Water Temperature at 10cm depth (ρ = 0.222)
6. Hydraulic Conductivity (ρ = 0.204)
7. FCO2 xmap Ecosystem Respiration[1] (ρ = 0.200)
8. Photosynthetic Radiation (ρ = 0.198)
9. Water Temperature at 30cm depth (ρ = 0.195)
10. FCO2 xmap FH2O Vapor[1] (ρ = 0.183)
11. Soil Temperature at 32cm depth (ρ = 0.164)
12. Air Pressure (ρ = 0.158)
13. Soil Temperature at 0cm depth (ρ = 0.152)
14. Ecosystem Respiration (ρ = 0.149)
15. Soil Temperature at 16cm depth (ρ = 0.137)
16. Soil Temperature at 8cm depth (ρ = 0.136)
17. Water Table Height (ρ = 0.119)
18. H2O Vapor Density (ρ = 0.107)
19. Dissolved Oxygen (ρ = 0.0363)
20. Vegetation Index (ρ = 0.00)

Seasonal. The strongest biophysical causal relationships regarding FCO2 at the seasonal scale were from Ecosystem Respiration to FCO2, Soil Temperature at 0 cm below the soil's surface to FCO2, Water Temperature at 10 cm below the soil's surface to FCO2, and FCH4 to FCO2.

1. Ecosystem Respiration ($\rho = 0.956$)
2. Soil Temperature at 0cm depth ($\rho = 0.908$)
3. Water Temperature at 10cm depth ($\rho = 0.890$)
4. FCH4 ($\rho = 0.880$)
5. Air Temperature ($\rho = 0.874$)
6. Air Pressure ($\rho = 0.871$)
7. Vapor Pressure Deficit ($\rho = 0.835$)
8. Soil Temperature at 16cm depth ($\rho = 0.779$)
9. FCO2 xmap FH2O Vapor[1] ($\rho = 0.763$)
10. FCO2 xmap Ecological Respiration[1] ($\rho = 0.726$)
11. Soil Temperature at 32cm depth ($\rho = 0.685$)
12. Soil Temperature at 8cm depth ($\rho = 0.671$)
13. FH2O Vapor ($\rho = 0.615$)
14. Water Temperature at 30cm depth ($\rho = 0.604$)
15. H2O Vapor Density ($\rho = 0.546$)
16. Water Table Height ($\rho = 0.302$)
17. Hydraulic Conductivity ($\rho = 0.136$)
18. Dissolved Oxygen ($\rho = 0.0681$)
19. Vegetation Index ($\rho = 0.00$)
20. Photosynthetic Radiation ($\rho = -0.0725$)

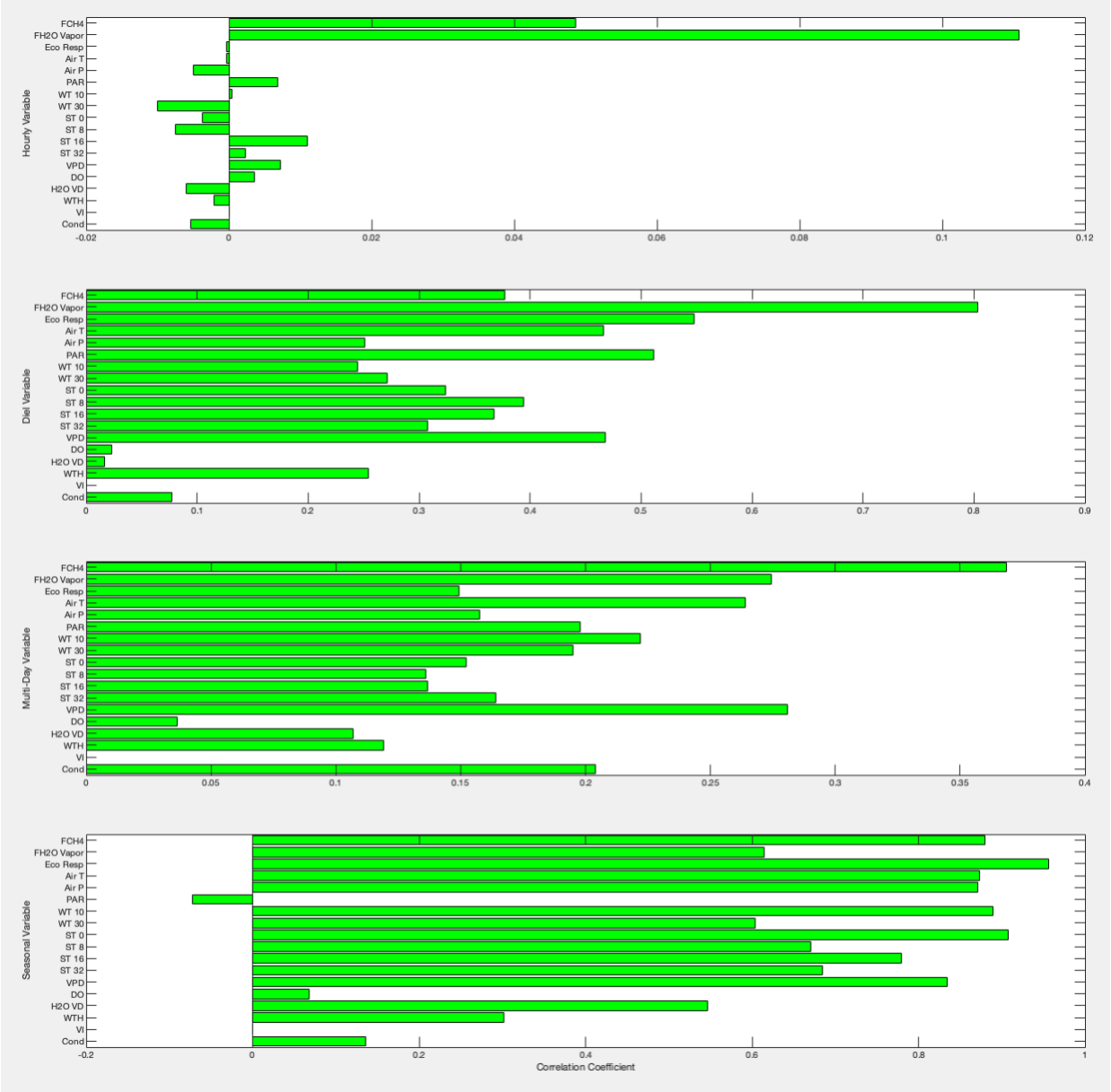

Figure 4. Causal Capacity of Contending Variables on FCO2. Applied rEDM package on contending biophysical drivers of FCH4. Cross Mapping Skill (ρ) represents correlation coefficients index (0-1). The closer ρ is to 1 is indicative of how much information from variable Y is stored in variable X, and thus how well X can predict Y, quantifying the level of causality from Y to X (Sugihara et al. 2012).

DISCUSSION

To improve the accuracy of climate model predictions with respect to the effects of future climate change on greenhouse gas emissions, this study aimed to uncover and quantitatively compare the biophysical variables that influence FCH4 and FCO2 in a tidal wetland ecosystem by the application of two statistical approaches in succession: (1) wavelet-based decomposition and (2) convergent cross mapping. With respect to FCH4 in the Hill Slough Wetland, the following variables had the highest forcing capacity on methane flux at the (a) hourly, (b) diel, (c) multi-day, and (d) seasonal scale: (a,c) water vapor flux and (b,d) carbon dioxide flux. Analogously, the following variables had the highest forcing capacity on carbon dioxide flux: (a,b) water vapor flux, (c) methane flux, and (d) ecosystem respiration.

For a majority of the computed signals, the cross mapping skill coefficients, which quantify the extent to which one variable influences another (based on the proximity of the CCM prediction compared to the actual signal), were comparatively larger for seasonal time scales, than for the shorter time scales. In addition, various computed signals in the hourly scale for FCH4, and in the hourly and seasonal scales for FCO2, resulted in negative values of the coefficients, signifying that portions of the predicted signal were opposite in sign to corresponding portions of the actual signal, which can further indicate an inaccurate input value for the time-lag specifically associated with the causal relationship in question (Martin et al. 2019).

Bi-directional forcing

With respect to bi-directional forcing (besides that between FCH4 and FCO2), only water vapor flux and ecosystem respiration exhibited forcing towards both FCH4 and FCO2. At the hourly scale, the results indicate a slightly stronger forcing from both FCH4 ($\rho = 0.179$) and FCO2 ($\rho = 0.146$) to water vapor flux, than in the direction from water vapor flux to both FCH4 ($\rho = 0.130$) and FCO2 ($\rho = 0.111$). At the diel scale, the greatest overall forcing capacity was from FCO2 towards water vapor flux ($\rho = 0.816$). At the seasonal scale, the largest overall forcing capacity was exhibited by FCH4 towards water vapor flux ($\rho = 0.927$). Overall, the results suggest a strong forcing capacity on all time scales from FCH4 to water vapor flux, as

well as from FCO2 to water vapor flux at hourly and diel scales. When considering the strong influence of water vapor flux in the direction of both FCH4 and FCO2, this would indicate the presence of a strong bi-directional feedback.

FCH4

FH2O vapor

Water vapor flux had the highest influence on methane flux at hourly ($\rho = 0.130$) and multi-day ($\rho = 0.500$) time scales, and was among the variables of highest influence at the diel ($\rho = 0.355$) and seasonal ($\rho = 0.838$) scales. Given the following indirect mechanisms and supporting literature explaining the coupling of water vapor flux and FCH4 (e.g., Bansal et al. 2020, Angle et al. 2016), there is greater plausibility in these findings as they correspond to bidirectional forcing of these two fluxes. An analogous study, using wavelet decomposition to isolate time scales of variation, in conjunction with mutual information as a means of causal analysis, found water vapor flux to be indicative of evapotranspiration having greater influence on FCH4 at hourly, diel, and multi-day (in the absence of strong water table variation) scales (Sturtevant et al. 2016). This study was also conducted in a non-tidal wetland in the same San Joaquin-Sacramento River Delta region.

During evapotranspiration, the lacunar air ventilation system in wetland vegetation that allows the transport of oxygen to the rhizosphere (narrow region of soil influenced by microorganisms that produce or oxidize CH4), also allows porewater CH4 to diffuse directly from the rhizosphere to the atmosphere (Bansal et al. 2020). The coupling of water vapor flux and FCH4 can be explained by the following indirect relationship: increased water vapor flux is indicative of increased radiation, as well as evapotranspiration, which further indicates increased photosynthesis, which provides the necessary substrate for methanogenesis, the process of anaerobic respiration which produces CH4 (Rinne et al. 2018). Given that methanogenesis was estimated to account for 80% of FCH4 in oxygenated wetland soils (Angle et al. 2016), in along with the diffusion of porewater CH4 to the atmosphere during evapotranspiration, there is greater plausibility of a causal relationship between water vapor flux and FCH4.

Microorganisms in Methane Modulation

However, there is controversy regarding whether soil-water characteristics dominate control over FCH4 in wetland ecosystems. With soil temperature and water temperature as parameters of soil-water characteristics, my study found soil and water temperature to have, on average, relatively less influence on FCH4 at all hourly (ρ = -0.003 for soil; ρ = 0.007 for water), diel (ρ = 0.104 for soil; ρ = 0.053 for water) and multi-day (ρ = 0.197 for soil ; ρ = 0.104 for water) time-scales, in comparison to the seasonal scale (ρ = 0.805 for soil; ρ = 0.840 for water). Other studies have consistently reported soil temperature and water temperature to dominate seasonal variation in methane emissions (Zhu et al. 2021; Chadburn et al. 2020), which could be due to soil temperature modulating the productivity and growth rates of methanogens (microorganisms that produce CH4) and methanotrophs (microorganisms that oxidize CH4) (Schütz et al. 1990). Therefore microbial dynamics are likely a strong influence on the seasonal cycle of wetland methane emissions, as the pathways of producing CH4 or oxidizing CH4 are more influenced by soil and water temperature at seasonal scales, than at shorter time scales. Furthermore, CH4 cycling microorganisms are influenced by the soil's hydrologic conditions, with methane producers being restricted to soils of higher moisture (Maietta et al. 2020). With hydraulic conductivity as a parameter of soil saturation, I found hydraulic conductivity to have the highest influence on FCH4 at the multi-day scale (ρ = 0.259), relative to all other time scales (seasonal: ρ = 0.0231, diel: ρ = 0.0276, hourly: ρ = -0.00881). Given that soils that experience prolonged periods of saturation support a high abundance of methanogens (Maietta et al. 2020), and thus significant FCH4, one can infer that a multi-day period of prolonged saturation supports optimum soil conditions for methanogens.

The highest driver of FCH4 at the seasonal scale was from FCO2 (ρ = 0.926), and closely followed by air temperature (ρ = 0.920). Degradation of soil organic carbon to methanogenic substrates (e.g., H2, CO2, acetate) is arguably the rate-limiting step in the production of CH4 (Conrad 2020). Given that methanogens and methanotrophs can be affected by limiting nutrients in wetland soils, and that CO2 is conducive to CH4 production, this would support the reasoning behind FCO2 having the highest influence on FCH4 at the seasonal scale.

Similarly, seasonal variations in CH4 emissions from a wide range of ecosystems have exhibited an average temperature dependence similar to that of CH4 production derived from pure cultures of methanogens (Yvon-Durocher et al. 2014). Thus we can infer that the consistent temperature dependence of CH4 emissions is most prominent at the seasonal scale. Given the time scale of causality, one can infer that CO2 as the limiting nutrient in CH4 production, as well as the ambient temperature effect on rates of reaction, are most apparent at longer time scales.

Water table is an additional parameter that has been shown to modulate FCH4, with increases in fluctuation correlating with increases in FCH4 (Yuan et al. 2021). My findings with respect to water table's influence on FCH4 were highest at the seasonal scale (seasonal: ρ = 0.113, multi-day: ρ = 0.112, diel: ρ = 0.085, hourly: ρ = -0.003). However, relative to the other contending variables, water table did not have a notable influence on FCH4, which could be due to either a sub-optimal value for time lag which would inhibit the CCM's ability to capture the appropriate time-lagged influence, or possible failure modes with respect to the signal's processing under CCM.

In conclusion, at shorter timescales FCH4 is predominantly influenced by evapotranspiration, at the multi-day scale FCH4 is driven by soil hydrological conditions that enable an abundant population of CH4 producing microorganisms. Lastly, at the seasonal scale FCH4 is influenced by FCO2, as increased carbon dioxide flux into soils enables optimal nutrient soil profile for CH4 production or oxidation by microorganisms, as well as air temperature due to the temperature dependence of methanogenesis (methane production).

FCO2

FH2O Vapor

Water vapor flux had the highest influence on carbon dioxide flux at hourly (ρ = 0.111) and diel (ρ = 0.803) time scales. Given the consistent documentation in the literature of FCO2 influence from vegetation above-ground biomass, there is a greater support in my findings as they correspond to the coupling of water vapor flux and FCO2, via the indirect mechanisms that account for plant growth regulating evapotranspiration.

Because the stomata (micropores in the epidermis of a leaf or plant stem) regulate the entry and exit of water vapor and CO2, stomata are not only the key to the assessment of evapotranspiration and water balance (represented by water vapor flux), but are also important for the estimation of FCO2 (Zha et al. 2013).

FCH4 had the highest influence on FCO2 at the multi-day scale ($\rho = 0.369$) and ecosystem respiration has the highest influence at the seasonal scale ($\rho = 0.956$). The proposed mechanisms behind these results are interconnected, considering how methanotrophs oxidize CH4 to CO2, utilizing the oxygen supplied to the rhizosphere from ecosystem respiration, which itself also produces CO2 (Bansal et al. 2020). Oxygen availability and diffusivity in wetlands are controlling factors for the production and consumption of both CO2 and CH4 in the subsoil, and hence, control the potential emission of these greenhouse gasses to the atmosphere (Elberling et al. 2011). Increased FCH4, associated with CH4 soil-uptake, would then enable increased levels of FCO2 to the atmosphere from CH4 oxidation, and can then be inferred as the primary control of FCO2 at multi-day scales. With respect to ecological respiration influencing FCO2 at the seasonal scale, the absence of plant above-ground biomass, or vegetation foliage, increases CO2 emissions, as reduction in vegetation results in greater rates of ecosystem respiration relative to photosynthesis (Yu et al. 2022; Olsson et al. 2015), which promotes CO2 emissions. Because ecosystem respiration comprises a major portion of total FCO2, one can infer that vegetation characteristics, at longer time scales, are the primary control of ecosystem respiration, and thus also of FCO2.

Vapor pressure deficit also had a high influence on FCO2 at multi-day ($\rho = 0.281$) and seasonal ($\rho = 0.835$) timescales. The proposed explanation for this control of FCO2 exemplifies the multifaceted, non-linear mechanisms of gas exchange at the plant-atmosphere interface: surface conductance (heat transmitted from a surface to the fluid in contact with the surface, or vice versa) was more sensitive to vapor pressure deficit under high radiation, leading to increased water vapor flux from transpiration, except when there was soil water deficiency in midsummer leading to a lower and constant surface conductance, thereby reducing transpiration (Zha et al. 2013).

In conclusion, with respect to the processes that modulate FCO2 across wetlands, a common theme is rooted in associated plant-atmosphere interactions. At the hourly and diel scale water vapor flux corresponds to rates of evapotranspiration, as well as vapor pressure deficit (at

longer time scales) directly corresponding to the surface conductance, and thus evapotranspiration. At multi-day and seasonal scales, FCH4 and ecosystem respiration, as the primary controls of FCO2, correspond to plant-mediated availability and diffusivity of oxygen as a limiting step in multiple CO2 production pathways.

Limitations of time series analysis

The discrepancies between previous findings for FCH4 specifically and results derived from wavelet decomposition and CCM here is most likely attributable to a combination of failure cases in which the CCM algorithm may falsely predict and/or detect causality. MODWT-based wavelet decomposition is deemed as an effective approach for revealing time-dependent variations and phases in the data (Yaacob et al. 2021). Because signal processing via wavelet time-scale decomposition has shown reliable performance for decomposing nonstationary FCH4 signals (Knox et al., 2018, 2021; Chamberlain et al., 2018; Sturtevant et al., 2016), it is less likely to be a sourcepoint of error, or consist of a relatively smaller portion of the inaccuracies in overall state space reconstruction in comparison to the CCM analysis. However, a notable limitation of using wavelet analysis surrounds the decomposed time scales that are subject to a scaling factor of 2^n, which may not necessarily correspond to ecological scales (Sturtevant et al. 2016).

Failure cases

CCM may not be as robust in its ability to discern causal dynamics in the context of performing ecological state space reconstruction, when considering the following possible failure modes: (1) nonreverting continuous dynamics, (2) synchrony, (3) integer multiple periods, (4) pathological symmetry, and (5) process noise (Yuan and Shou 2022). Given that CCM detects a continuous delay map between two variables (X and Y) and uses this to infer the presence and direction of causation, in the first failure mode, a continuous map might be found from the delay space of X to time and from time to Y, which falsely assumes causality from X to Y when there is a clear temporal trend among the two variables (Yuan and Shou 2022). In the second case, when the coupling is so strong that it results in synchronization of variables X and Y,

bidirectional causality may be inferred when it is unidirectional (Mønster et al. 2017). In the third case, when X's period, or length of complete cycle, is an integer multiple of Y's period, Y may be predicted to cause X when there is no causal relation (Yuan and Shou 2022). In the fourth failure case, when there is persistent symmetry CCM fails to predict bidirectional causality (Yuan and Shou 2022). In the case of process noise (discordant data that may arise from natural variation and stochastic processes), for higher levels of noise CCM correlations drop linearly as a function of added noise, and the rate of convergence becomes a more robust indicator of causality (Mønster et al. 2017). Because convergence is yet to be a well-defined quantifiable parameter in the literature, this lack of definitive measure poses an issue for determining causality based solely on the rate of convergence. It is essential to account for these CCM failure modes when considering the legitimacy of CCM as a statistical tool for ecological data analysis.

Moreover, time-lag is one of the two parameters that have a significant influence on the CCM algorithm's output accuracy (Mønster et al. 2017). Because the time lag was only set to a default value of -1, and plausibly not the optimal value for each pair-wise computation, this default setting of time lag can account for an underestimation or overestimation in causality. Therefore, for future studies, it is recommended to procure the optimal time lag and embedding dimension for each pair-wise computation.

Implications

Wavelet decomposition is a reliable statistical method for data analysis at isolated frequencies. However, further investigation of CCM and similar statistical algorithms that test for causality in non-deterministic systems is essential to consistently and accurately identify and quantify causal relationships in ecological systems.

The differences in CCM correlation coefficients among timescales for each respective pair-wise analysis highlights the importance of including properties of scale for comprehensively understanding causality and accurately predicting the interactions between FCH4 and FCO2 and their biophysical controls.

Although the causal associations regarding water vapor flux and carbon dioxide flux for FCH4, and water vapor flux, methane flux, and ecosystem respiration for FCO2 were consistent

with previous conclusions, further investigation on the biophysical controls of trace gas exchange across different biomes is necessary to better formulate global circulation models.

ACKNOWLEDGMENTS

I would like to especially thank Patina Mendez for her steadfast support in navigating my first research project, as well as my workgroup peers for their constructive insights and thoughtful suggestions. I am very grateful for the enormous amount of time and consideration it took to give feedback. I would also like to thank Dennis Baldocchi, for the incredible opportunity to do this analytical work that aligns so closely with my interests. I have learned much more than I could have imagined, during this effort to bridge the gap between quantitative analysis in understanding bio-ecological processes. I would also like to thank Kyle Delwiche for her support in navigating the nuances of wavelet decomposition and convergent cross mapping. I truly appreciate all that I have learned from our collaborations. Lastly, I would like to thank Ariane Arias Ortiz for her guidance and direction throughout these investigations. This project has been extremely rewarding, and I hope that this work can be useful for future investigations in the natural sciences.

REFERENCES

Angle, J. C., T. H. Morin, L. M. Solden, A. B. Narrowe, G. J. Smith, M. A. Borton, C. Rey-Sanchez, R. A. Daly, G. Mirfenderesgi, D. W. Hoyt, W. J. Riley, C. S. Miller, G. Bohrer, and K. C. Wrighton. 2017. Methanogenesis in oxygenated soils is a substantial fraction of wetland methane emissions. Nature Communications 8:1567.

Arias-Ortiz, A., P. Y. Oikawa, J. Carlin, P. Masqué, J. Shahan, S. Kanneg, A. Paytan, and D. D. Baldocchi. 2021. Tidal and Nontidal Marsh Restoration: A Trade-Off Between Carbon Sequestration, Methane Emissions, and Soil Accretion. Journal of Geophysical Research: Biogeosciences 126.

Bansal, S., O. F. Johnson, J. Meier, and X. Zhu. 2020. Vegetation Affects Timing and Location of Wetland Methane Emissions. Journal of Geophysical Research: Biogeosciences 125.

Callaway, J. C., E. L. Borgnis, R. E. Turner, and C. S. Milan. 2012. Carbon Sequestration and Sediment Accretion in San Francisco Bay Tidal Wetlands. Estuaries and Coasts 35:1163–1181.

Cazelles, B., M. Chavez, D. Berteaux, F. Ménard, J. O. Vik, S. Jenouvrier, and N. C. Stenseth. 2008. Wavelet analysis of ecological time series. Oecologia 156:287–304.

Cao, Z., S. Mu, L. Xu, M. Shao, and H. Qu. 2021. Causal Research on Soil Temperature and Moisture Content at Different Depths. IEEE Access 9:39077–39088.

Chadburn, S. E., T. Aalto, M. Aurela, D. Baldocchi, C. Biasi, J. Boike, E. J. Burke, E. Comyn-Platt, A. J. Dolman, C. Duran-Rojas, Y. Fan, T. Friborg, Y. Gao, N. Gedney, M. Göckede, G. D. Hayman, D. Holl, G. Hugelius, L. Kutzbach, H. Lee, A. Lohila, F. W. Parmentier, T. Sachs, N. J. Shurpali, and S. Westermann. 2020. Modeled Microbial Dynamics Explain the Apparent Temperature Sensitivity of Wetland Methane Emissions. Global Biogeochemical Cycles 34.

Chamberlain, S. D., T. L. Anthony, W. L. Silver, E. Eichelmann, K. S. Hemes, P. Y. Oikawa, C. Sturtevant, D. J. Szutu, J. G. Verfaillie, and D. D. Baldocchi. 2018. Soil properties and sediment accretion modulate methane fluxes from restored wetlands. Global Change Biology 24:4107–4121.

Clark, A. T., H. Ye, F. Isbell, E. R. Deyle, J. Cowles, G. D. Tilman, and G. Sugihara. 2015. Spatial convergent cross mapping to detect causal relationships from short time series. Ecology 96:1174–1181.

Conrad, R. 2020. Methane Production in Soil Environments—Anaerobic Biogeochemistry and Microbial Life between Flooding and Desiccation. Microorganisms 8:881.

De Deyn, G. B., J. H. C. Cornelissen, and R. D. Bardgett. 2008. Plant functional traits and soil carbon sequestration in contrasting biomes. Ecology Letters 11:516–531.

Elberling, B., L. Askaer, C. J. Jørgensen, H. P. Joensen, M. Kühl, R. N. Glud, and F. R. Lauritsen. 2011. Linking Soil O 2 , CO 2 , and CH 4 Concentrations in a Wetland Soil: Implications for CO 2 and CH 4 Fluxes. Environmental Science & Technology 45:3393–3399.

Huntingford, C., J. A. Lowe, N. Howarth, N. H. A. Bowerman, L. K. Gohar, A. Otto, D. S. Lee, S. M. Smith, M. G. J. den Elzen, D. P. van Vuuren, R. J. Millar, and M. R. Allen. 2015. The implications of carbon dioxide and methane exchange for the heavy mitigation RCP2.6 scenario under two metrics. Environmental Science & Policy 51:77–87.

Knox, S. H., L. Windham-Myers, F. Anderson, C. Sturtevant, and B. Bergamaschi. 2018. Direct and Indirect Effects of Tides on Ecosystem-Scale CO 2 Exchange in a Brackish Tidal Marsh in Northern California. Journal of Geophysical Research: Biogeosciences 123:787–806.

Knox, S. H., S. Bansal, G. McNicol, K. Schafer, C. Sturtevant, M. Ueyama, A. C. Valach, D. Baldocchi, K. Delwiche, A. R. Desai, E. Euskirchen, J. Liu, A. Lohila, A. Malhotra, L. Melling, W. Riley, B. R. K. Runkle, J. Turner, R. Vargas, Q. Zhu, T. Alto, E. Fluet-Chouinard, M. Goeckede, J. R. Melton, O. Sonnentag, T. Vesala, E. Ward, Z. Zhang, S. Feron, Z. Ouyang, P. Alekseychik, M. Aurela, G. Bohrer, D. I. Campbell, J. Chen, H. Chu, H. J. Dalmagro, J. P. Goodrich, P. Gottschalk, T. Hirano, H. Iwata, G. Jurasinski, M. Kang, F. Koebsch, I. Mammarella, M. B. Nilsson, K. Ono, M. Peichl, O. Peltola, Y. Ryu, T. Sachs, A. Sakabe, J. P. Sparks, E. Tuittila, G. L. Vourlitis, G. X. Wong, L. Windham-Myers, B. Poulter, and R. B. Jackson. 2021. Identifying dominant environmental predictors of freshwater wetland methane fluxes across diurnal to seasonal time scales. Global Change Biology 27:3582–3604.

Li, Q., S. Gogo, F. Leroy, C. Guimbaud, and F. Laggoun-Défarge. 2021. Response of Peatland CO2 and CH4 Fluxes to Experimental Warming and the Carbon Balance. Frontiers in Earth Science 9:631368.

Liu, Y. 2021. Analysis on the Influencing Factors of Methane Emission from Wetlands. IOP Conference Series: Earth and Environmental Science 943:012006.

Liu, J., A. Valach, D. Baldocchi, and D. Y. F. Lai. 2022. Biophysical Controls of Ecosystem-Scale Methane Fluxes From a Subtropical Estuarine Mangrove: Multiscale, Nonlinearity, Asynchrony and Causality. Global Biogeochemical Cycles 36.

Maietta, C. E., K. L. Hondula, C. N. Jones, and M. A. Palmer. 2020. Hydrological Conditions Influence Soil and Methane-Cycling Microbial Populations in Seasonally Saturated Wetlands. Frontiers in Environmental Science 8:593942.

Martin, R., J. Koo, and D. Eckhardt. 2019, March 7. Impact of Embedding View on Cross Mapping Convergence. arXiv.

The MathWorks Inc. 2020b. MATLAB version: 9. 9. 0. (R2020b). Natick, Massachusetts, United States.

Mønster, D., R. Fusaroli, K. Tylén, A. Roepstorff, and J. F. Sherson. 2017. Causal inference from noisy time-series data — Testing the Convergent Cross-Mapping algorithm in the presence of noise and external influence. Future Generation Computer Systems 73:52–62.

Olsson, L., S. Ye, X. Yu, M. Wei, K. W. Krauss, and H. Brix. 2015. Factors influencing CO and CH emissions from coastal wetlands in the Liaohe Delta, Northeast China. Biogeosciences 12:4965–4977.

Prieto-Guerrero, A., and G. Espinosa-Paredes. 2019. Linear signal processing methods and decay ratio estimation. Pages 269–314 Linear and Non-Linear Stability Analysis in Boiling Water Reactors. Elsevier.

Rinne, J., E.-S. Tuittila, O. Peltola, X. Li, M. Raivonen, P. Alekseychik, S. Haapanala, M. Pihlatie, M. Aurela, I. Mammarella, and T. Vesala. 2018. Temporal Variation of Ecosystem Scale Methane Emission From a Boreal Fen in Relation to Temperature, Water Table Position, and Carbon Dioxide Fluxes. Global Biogeochemical Cycles 32:1087–1106.

RStudio Team. 2020. R Version 2021.09.2. RStudio: Integrated Development for R. Boston, Massachusetts, United States.

Schütz, H., W. Sieler, and R. Conrad. 1990. Influence of Soil Temperature on Methane Emission from Rice Paddy Fields. Biogeochemistry 11:77–95.

Sturtevant, C., B. L. Ruddell, S. H. Knox, J. Verfaillie, J. H. Matthes, P. Y. Oikawa, and D. Baldocchi. 2016. Identifying scale-emergent, nonlinear, asynchronous processes of wetland methane exchange. Journal of Geophysical Research: Biogeosciences 121:188–204.

Sugihara, G., R. May, H. Ye, C. Hsieh, E. Deyle, M. Fogarty, and S. Munch. 2012. Detecting Causality in Complex Ecosystems. Science 338:496–500.

Valach, A. C., K. Kasak, K. S. Hemes, T. L. Anthony, I. Dronova, S. Taddeo, W. L. Silver, D. Szutu, J. Verfaillie, and D. D. Baldocchi. 2021. Productive wetlands restored for carbon sequestration quickly become net CO2 sinks with site-level factors driving uptake variability. PLOS ONE 16:e0248398.

Windham-Myers, L., E. Stuart-Haëntjens, B. Bergamaschi, and S. Knox. 2020. FLUXNET-CH4 US-Srr Suisun marsh - Rush Ranch. FluxNet; United States Geological Survey; USGS.

Yaacob, N. A., J. J. Jaber, D. Pathmanathan, S. Alwadi, and I. Mohamed. 2021. Hybrid of the Lee-Carter Model with Maximum Overlap Discrete Wavelet Transform Filters in Forecasting Mortality Rates. Mathematics 9:2295.

Yu, B., W. Xu, L. Yan, H. Bao, and H. Yu. 2022. Spatial and Temporal Variability and Driving Factors of Carbon Dioxide and Nitrous Oxide Fluxes in Alpine Wetland Ecosystems. Plants 11:2823.

Yuan, A. E., and W. Shou. 2022. Data-driven causal analysis of observational biological time series. eLife 11:e72518.

Yvon-Durocher, G., A. P. Allen, D. Bastviken, R. Conrad, C. Gudasz, A. St-Pierre, N. Thanh-Duc, and P. A. del Giorgio. 2014. Methane fluxes show consistent temperature dependence across microbial to ecosystem scales. Nature 507:488–491.

Zha, T., C. Li, S. Kellomäki, H. Peltola, K.-Y. Wang, and Y. Zhang. 2013. Controls of Evapotranspiration and CO2 Fluxes from Scots Pine by Surface Conductance and Abiotic Factors. PLoS ONE 8:e69027.

Zhu, D., N. Wu, N. Bhattarai, K. P. Oli, H. Chen, G. S. Rawat, I. Rashid, M. Dhakal, S. Joshi, J. Tian, Q. Zhu, S. Chaudhary, and K. Tshering. 2021. Methane emissions respond to soil temperature in convergent patterns but divergent sensitivities across wetlands along altitude. Global Change Biology 27:941–955.

APPENDIX

Appendix A: Dutch Slough Wetland Wavelet Decomposition for 170 day time-series

Appendix B: Dutch Slough Wetland rEDM